Research of Power Inspection Based on Intelligent Algorithm

Lei Tian, Member, IAENG, Minhang Mao, Member, IAENG, Baoyu Hou, Gao Ma

***Abstract*—Manual methods involve a large workload and high risk in electric power inspections. Additionally, drone inspections are constrained by limited range, making inspecting areas with complex terrain difficult. Spurred by these limitations, this study proposes an integrated power inspection system that synergistically combines an inspection vehicle and a drone to confront these problems. The primary objective of this research is to establish a vehicle-mounted drone inspection system model and formulate an optimization goal using the total inspection distance as the objective function. Specifically, an improved ant colony optimization (IACO) algorithm is employed to optimize the solution, and the proposed multi-path selection mechanism and elite strategy improve the algorithm's performance. The results are compared against the original ant colony optimization (ACO) algorithm, dynamic evaporation rate adaptive ant colony optimization (DERAACO) algorithm, A* algorithm, and genetic algorithm on a city's transmission tower map and actual tower data. The simulation results indicate that the IACO significantly improves route planning efficiency, enhances operational efficiency, and validates the feasibility of the proposed vehicle-mounted drone inspection model. This research provides essential theoretical insights and practical implications for advancing electric power inspection methodologies.**

***Index Terms*—Path planning, Power inspection, Ant colony algorithm, Drone, Inspection vehicle**

I. INTRODUCTION

POWER grid is essential for maintaining the security and reliability of electricity provision, as well as harmonizing the equilibrium between energy generation and consumption across different areas [1-2]. The escalation in household power consumption, alongside the ongoing enlargement of the electrical grid's infrastructure, has markedly increased the demands for safeguarding the consistent and secure functioning of power networks.Power inspection has become a standard method of power maintenance. Traditional maintenance relies on manual inspections, which involve a large workload and face the complexity and dynamic nature of the inspected areas, posing numerous challenges for manual inspection. Considering both the safety of inspectors and the effectiveness of the inspection in a comprehensive manner, using drones and other intelligent devices for power autonomous inspection has become a new mode of power inspection [3-6], which significantly improves the efficiency of line inspection and reduces inspection risks. However, the complex terrain of the inspection, combined with the limited operating range of the drone, simply relying on the drone for inspection will cause a waste of resources. Consequently, a novel collaborative inspection mode has emerged, integrating an inspection vehicle and a drone.

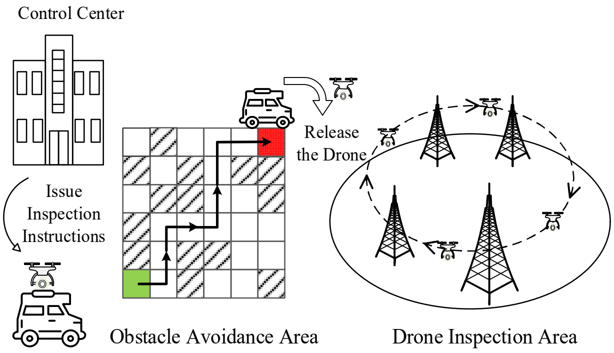

Fig. 1. Inspection Vehicle and Drone Collaborative Inspection

Currently, the literature offers several path-inspection methods in power inspection. For example, Chen et al. [7] optimized the robot inspection route based on a genetic algorithm and applied grid processing on the substation plan in the mobile robot inspection system. Lu et al. [8] proposed a path-planning method for electric emergency robots by combining the analytic hierarchy process (AHP) and the A* algorithm for global and local dynamic path planning, thereby avoiding operational risks. Based on the ant colony algorithm, Xie et al. [9] relied on the directional Angle factor and the Laplacian probability distribution function to significantly improve the robot's work efficiency in the inspection substation. For the study of vehicle and drone cooperative inspection, Huang et al. [10] developed a new mode of collaborative power detection of “UAV and operating vehicle (OV)”, which adopted an improved K-means algorithm and a genetic algorithm to solve the model. They also conducted a case analysis demonstrating the capability of their method. Zhao et al. [11] focused on the

Manuscript received January 7, 2024; revised February 11, 2025. This work was supported in the Key Research and Development Program of Shaanxi (Program No.2024GX-YBXM-033), the Natural Science Basic Research Program of Shaanxi (No. 2021JM-460), Xi'an University of Posts and Telecommunications Graduate Course Construction and Education and Teaching Reform Project (YJGJ2024039), the Scientific Research Program of Shaanxi Provincial Education Department (No. 21JC033), the Science and Technology Project of Xi'an city. (No. 22GXFW0126), the Innovation and Entrepreneurship Training Program for Undergraduate (No.202311664058).

Lei Tian is an associate professor at the School of Electronic Engineering, Xi’an University of Posts and Telecommunications, Xi’an 710121 China. (corresponding author to provide phone: +86-15929907626; e-mail: tianlei@xupt.edu.cn).

Minhang Mao is a postgraduate student at the School of Electronic Engineering, Xi’an University of Posts and Telecommunications, Xi’an 710121 China. (e-mail: maominhang_1@163.com).

Baoyu Hou is a project manager overseeing power distribution operations at the Quzhou Power Supply Branch, State Grid Zhejiang Electric Power Co. Ltd, Quzhou 324000, China (e-mail: tla02@126.com).

Gao Ma is a project manager specializing in space microwave technology at the CAST Xi’an Institute of Space Radio Technology, China Academy of Space Technology, Xi’an 710100, China. (e-mail: 364945696@qq.com)

TABLE I
SETS AND PARAMETERS

Symbol		Meaning
Set	S	the set of the control center, S={s_0}
	P	the set of parking points, P={p_0}
	O	the set of obstacle area, O={o_0}
	C	the set of inspection vehicles, C={c_0}
	D	the set of drones, D={d_0}
	T	the set of towers, T={t_1,t_2...t_m}
Parameter	L_C	the length of the inspection vehicle, km
	L_D	the length of the drone, m

km = kilometer, m =meter.

realization of UAVs and vehicles in time and space cooperation and proposed an integrated vehicle-mounted UAV cooperative operation mode based on a space-time network.

This study uses drones and inspection vehicles to complete cross-area inspections jointly. The inspection area is divided into different regions, and the developed method realizes reasonable obstacle avoidance routes in the vehicle-mounted drone inspection area, facilitating the optimization of the shortest path for the tower inspection task. The ant colony algorithm is employed to address this challenge effectively, which is a NP-hard problem, it can solve the problem faster and get a better solution [12-13]. The model is evaluated on a simulated problem to verify the distribution of transmission line towers in a city, followed by a thorough examination of the results. The proposed method offers a scientific and practical decision-making approach for power enterprises to devise reasonable path-planning schemes.

II. COLLABORATIVE INSPECTION MODE OF DRONE AND INSPECTION VEHICLE

A. Problem Description

Assuming a need for power inspection of transmission towers in a specific area, the inspection mode is illustrated in Fig. 1.

The power company utilizes inspection vehicles and drones in a collaborative power inspection mode, during which the inspection is divided into two areas. The first is the obstacle avoidance area for the inspection vehicles. In this area, the inspection process involves the deployment of a vehicle-mounted drone from the intelligent control center, which navigates through a complex obstacle environment that requires practical obstacle avoidance operations. The second is the drone inspection area. After passing the obstacle avoidance area, the inspection vehicle will park at the designated parking spot and release the drone by remote control to inspect the transmission tower. After completing the corresponding inspection task, the drone lands on the take-off and landing platform of the inspection vehicle, and along with the vehicle, they both return to the control center.

B. Problem Assumption

Based on the inspection of transmission towers and combined with the operation constraints of inspection equipment. In order to facilitate quantitative research and increase the understanding of the model, the following assumptions are made for the collaborative inspection model

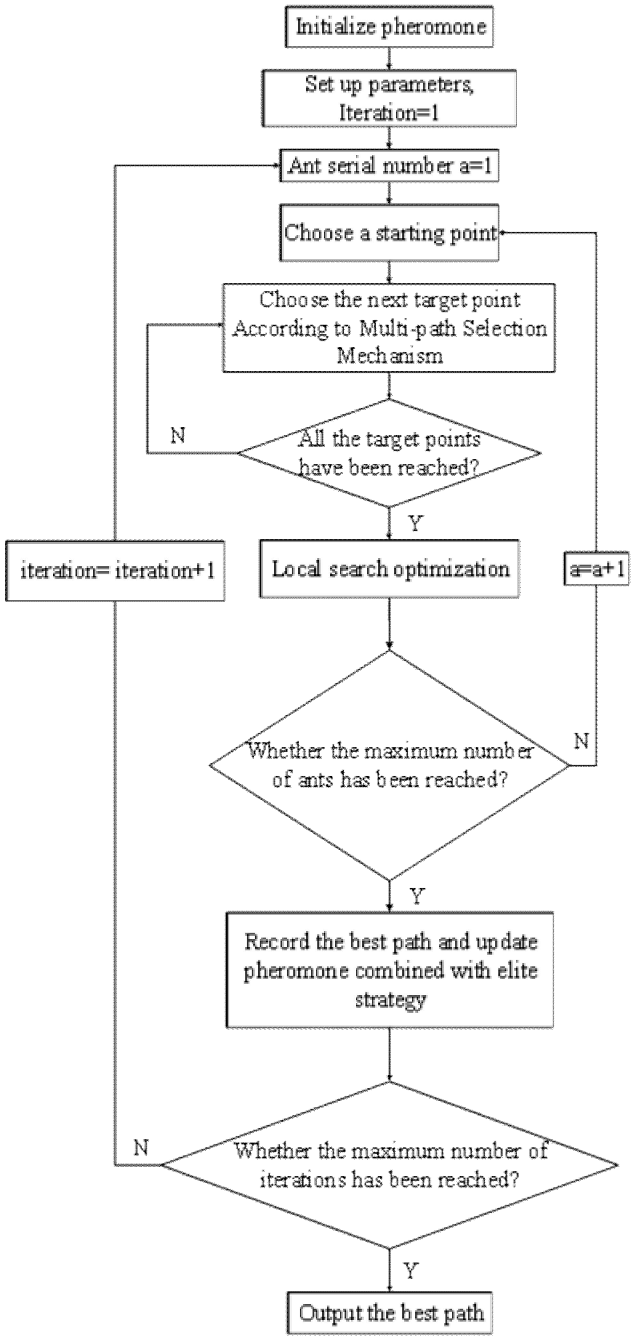

Fig. 2. Flowchart of the IACO Algorithm

of inspection vehicles and drones:

(1) Access hypothesis: Given that the distance between the operation and maintenance station and the power tower to be inspected significantly exceeds the farthest distance of a single flight of the drone, the drone must be transported by the inspection vehicle to the vicinity of the tower before initiating the inspection. Due to road restrictions, the inspection vehicle is only active from the operation and maintenance station to the docking point.

(2) Starting hypothesis of the control center: The inspection vehicle departs from the control center and waits for the drone to return to the control center after completing its inspection tasks.

(3) Path hypothesis: The path focuses on the sequence in which the drones visit the points to be inspected. It does not rely entirely on the exact locations of inspection towers or power grid points. The drone inspection path planning is simplified from a three-dimensional problem to a

TABLE II
POSITION COORDINATES OF 20 TOWERS IN A CITY

Tower number	(x, y)	Tower number	(x, y)
1	(220,55)	11	(538,87)
2	(367,314)	12	(764,320)
3	(382,409)	13	(806,293)
4	(413,526)	14	(917,462)
5	(320,611)	15	(987,216)
6	(178,784)	16	(625,509)
7	(515,703)	17	(782,735)
8	(571,600)	18	(811,784)
9	(605,414)	19	(929,690)
10	(631,223)	20	(958,525)

two-dimensional path optimization problem. Therefore, the distance traveled by the drone from one inspection point to the next is assumed to be a two-dimensional linear distance, which can be directly calculated using the Euclidean distance formula between two points. It can be obtained directly from the Euclidean distance formula between two points.

(4) Drone inspection hypothesis: Due to cost and practical constraints, the inspection vehicle is equipped with a single drone, capable of inspecting all towers in one trip. The drone's flying speed is assumed to be the same both during transit to and from the inspection area and between the towers. The inspection time at each tower is also considered to be the same. The drone must begin and end its flight at the same point, flying in a straight line between the inspection area and each tower, with the take-off and landing distances ignored for simplicity.

C. Model Construction

Table I reports some basic sets and parameters to clarify the subsequent description.

The total inspection path length can be calculated as follows:

$$f(L) = L_C + L_D \tag{1}$$

III. ALGORITHM DESIGN

Traditional path planning algorithms, such as the A* algorithm, have the advantage of quickly finding the optimal path. They can adapt to various terrains and obstacles based on heuristic functions. However, with the advancement of artificial intelligence algorithms, intelligent algorithms have shown superiority over traditional path-planning algorithms. For instance, the genetic algorithm, which simulates the genetic and evolutionary processes of biology in nature, exhibits characteristics of parallelism, high efficiency, and global search capabilities. Among the various path-planning algorithms, this paper utilizes the ant colony algorithm, owing to its excellent global search capability and potential parallelism, which is appropriate for solving path-planning problems. Dorigo first proposed the ant colony algorithm [14], which is a type of bionic swarm intelligence algorithm. Specifically, the optimal solution is constructed based on the ant's foraging behavior, i.e., when ants seek a path to feed, they release pheromones to record the current path. The probability that the ants choose the path is related to the pheromone concentration.

Fig. 3. Transmission Towers Map

A. Obstacle Avoidance Path Planning Algorithm for Inspection Vehicle

It is necessary to conduct environmental modeling according to obstacle avoidance path planning characteristics [15]. For environmental modeling, this study adopts a structured discretization approach based on grid decomposition. The grid-based modeling approach was selected for its computational practicality, combining intuitive spatial representation with efficient algorithmic implementation. The grid map is constituted by a matrix of 0s and 1s, where 0 represents a free grid that the inspection vehicle can pass through, while 1 denotes an obstacle grid that the vehicle cannot traverse. The sequence number method is typically applied when the grid method is used to build the environment model and transform the environmental information into identifiable information. Each smallest square of the grid map is added in numbered order until the last square is identified.

Each grid in a grid map has a corresponding number, with the following formula expressing the coordinates of the different sequence grids in the coordinate system:

$$\begin{cases} x_i = a(mod(i, N_x) - 0.5) \\ y_i = a(N_y + 0.5 - ceil(i / N_y)) \end{cases} \tag{2}$$

where a denotes grid resolution, *mod* means complementary operation, ceil stands for integer up operation. The position of the i_{th} grid is defined as (x_i, y_i), with N_x and N_y representing row/column grid counts respectively. The length of each complete path is calculated as follows:

$$D_{i,j} = \sqrt{(x_i - x_j)^2 + (y_i - y_j)^2} \tag{3}$$

When designing the motion method, it is necessary to determine the strategy for changing route direction. We adopt an eight-way turning strategy, i.e., during the path search process, the path can turn in any of the eight directions. While turning, it is crucial to determine whether the adjacent grids around the current grid are obstacles or open grids. Thus, a matrix D is introduced to represent the adjacency of the grids and whether they are obstacles. Matrix D records the transition values between each grid point and its neighboring one. The grid map established comprises 20×20 grid points; thus, the size of matrix D is 400×400. The value from each

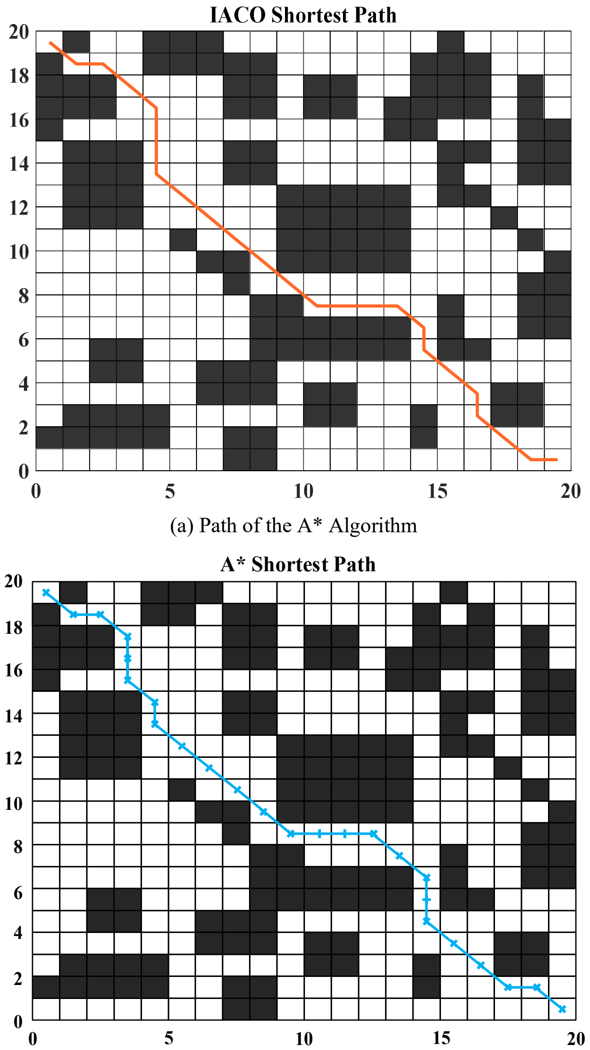

(a) Path of the A* Algorithm

(b) Path of IACO

Fig. 4. Inspection Vehicle Path Results

grid point to its neighboring obstacle-free grid points is set to 1, while the value to obstacle grids or non-neighboring grids is set to 0.

B. Path Planning Algorithm for Inspection Drone

The drone inspection path adopts the shortest path algorithm to solve the traversal inspection. Since the order of the inspection points affects the distance length of the path, we employ the Traveling Salesman Problem (TSP) solution in the ant colony algorithm to find the shortest path [16]. The traveling salesman problem states that if a traveling businessman wants to visit n cities, he needs to choose a route that passes from all cities back to the starting point while minimizing the distance covered. This method utilized to address this issue is delineated in the following manner:

For spatial modeling, the Euclidean distance between any two nodes i and j within the set $S=\{1,2,...,n\}$ is defined as:

$$d_{i,j} = \sqrt{(x_i - x_j)^2 + (y_i - y_j)^2} \tag{4}$$

Each ant maintains a dynamic tabu list to store its traversal history. The initial entry in this list corresponds to the ant's starting position. As the ant navigates through the environment, it sequentially appends visited points to the list. Traversal completion is achieved when the tabu list contains all target points. Following the colony's exploration from iteration t to $t+n$, the pheromone concentration on the path connecting points i and j at iteration $t+n$ is updated as follows:

TABLE III
COMPARISON OF EXPERIMENTAL RESULTS

Algorithms	Minimum distance/km	Iterations	Turn times
A*	29.8	122	12
IACO	29.5	24	11

$$a_{ij}(t+n) = (1-\rho) \times a_{ij}(t) + \Delta a_{ij} \tag{5}$$

The pheromone level $a_{ij}(t)$ between points i and j is initialized to a predefined constant. The update mechanism incorporates a volatilization factor ρ ($0 \leq \rho \leq 1$), which governs the rate of pheromone decay between iterations t and $t+n$. The term ($1-\rho$) quantifies the residual pheromone retention, while Δa_{ij} captures the incremental pheromone deposition during this interval, computed as:

$$\Delta a_{ij} = \sum_{k=1}^{m} \Delta a_{ij}{}^{k} \tag{6}$$

where $\Delta a_{ij}{}^{k}$ represents the pheromone increment of the k_{th} ant on the path from i to j during this iteration, calculated as follows using the ant cycle model:

$$\Delta a_{ij}{}^{k} = \begin{Bmatrix} Q/L_k, \text{ Ant } k \text{ goes from } i \text{ to } j \\ 0, \text{ Ant } k \text{ didn't go from } i \text{ to } j \end{Bmatrix} \tag{7}$$

where Q is a normal number, representing the ant's path in its journey. The advantage of the ant cycle model lies in its ability to incorporate pheromone information on a global scale.

The probabilistic transition mechanism governing ant movement at iteration t follows the rule:

$$p_{ij}^{k}(t) = \begin{Bmatrix} \dfrac{[a_{ij}(t)]^{\alpha} * [\eta_{ij}(t)]^{\beta}}{\sum_{S \in J_k(i)} [a_{ij}(t)]^{\alpha} * [\eta_{ij}(t)]^{\beta}}, \ j \in J_k(i) \\ 0, j \notin J_k(i) \end{Bmatrix} \tag{8}$$

where $\eta_{ij}(t)$ is a heuristic factor represented by a normal number, formulated as:

$$\eta_{ij}(t) = 1/d_{ij} \tag{9}$$

where η_{ij} represents the heuristic desirability of moving from point i to j, and $J_k(i)$ denotes the set of feasible neighboring points accessible to the k_{th} ant from its current position i. Parameters α and β modulate the relative weights of pheromone concentration and heuristic information, respectively, in the decision-making process.

C. Improved Ant Colony Optimization (IACO) Algorithm

1) Multi-path Selection Mechanism

According to the state selection probability, the ant moves to the next path point in the original ACO. As the number of iterations increases, ants tend to concentrate on selecting specific paths, which can result in the algorithm becoming trapped in a local optimum. Thus, introducing a multi-path selection mechanism based on path similarity can improve the algorithm's global search capability. Assuming that the

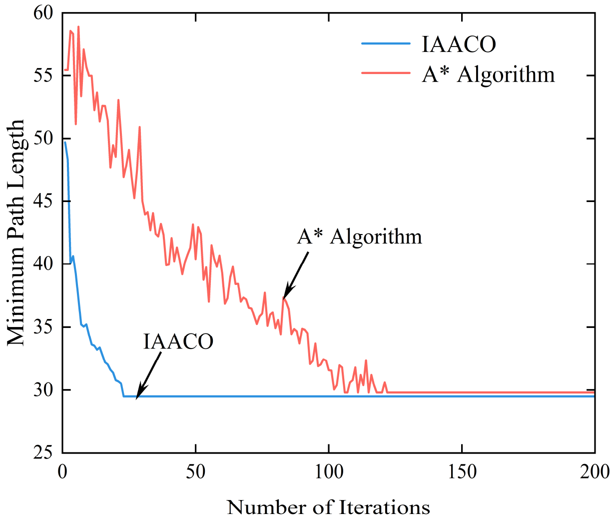

Fig. 5. Convergence Results

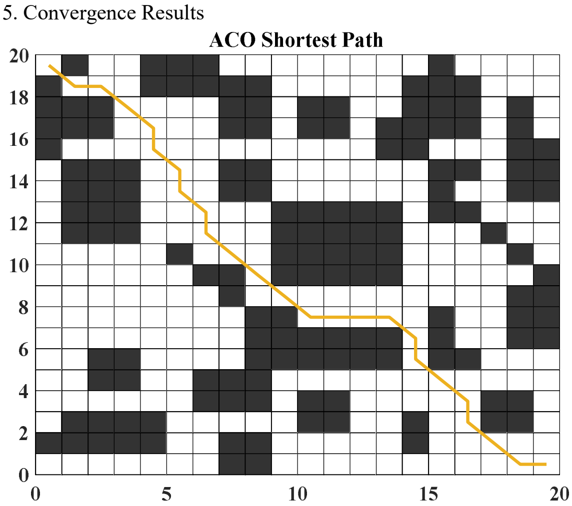

(a) Optimal Path Generated by Original ACO

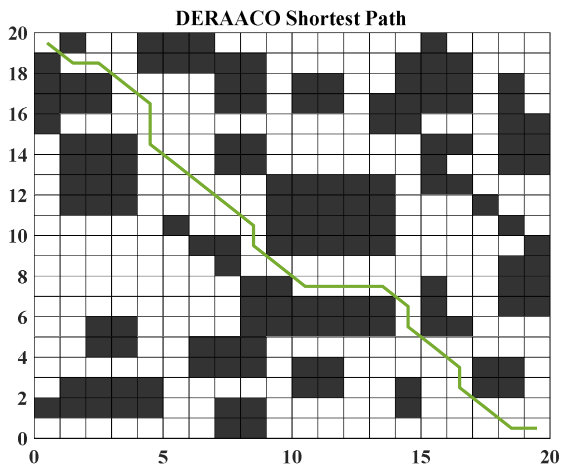

(b)Optimal Path Generated by DERAACO

Fig. 6. Optimal Path Generated by Different ACO Algorithms

route r^k of the current ant k has a certain similarity with the previously selected route r^m, the route similarity $sim(r^k,r^m)$ is defined as:

$$sim(r^k, r^m) = \frac{\sum_{i=1}^{L} 1\{r^k(i) = r^m(i)\}}{L} \tag{10}$$

where $r^k(i)$ and $r^m(i)$ represent the i_{th} node of routes r^k and r^m, L is the minimum length of the route, and $1\{r^k(i)= r^m(i)\}$ is the indicator function, which returns 1 if $r^k(i)= r^m(i)$, and 0 otherwise.

TABLE IV

EXPERIMENTAL RESULTS OF DIFFERENT ALGORITHMS

Algorithm	Path length			Convergence generation			Turn times
	Best	Mean	Std	Best	Mean	Std	
A*	29.80	29.80	0.00	-	-	-	12.00
ACO	29.50	31.87	0.95	23.00	25.30	0.93	15.00
DERAACO	29.50	30.04	0.66	47.00	49.00	0.89	13.00
IACO	29.50	29.50	0.0	18.00	18.33	0.22	11.00

The selection probability $p_{ij}^k(t)$ can be adjusted according to the path similarity to guide exploring different paths. The formula for the adjusted path selection probability is:

$$p_{ij}^k(t) = \frac{[a_{ij}(t)]^\alpha * [\eta_{ij}(t)]^\beta}{\sum_{S \in J_k(i)} [a_{ij}(t)]^\alpha * [\eta_{ij}(t)]^\beta} \times (1 - sim(r^k, r^m)) \tag{11}$$

where $(1\text{-}sim(r^k,r^m))$ reduces the likelihood of being similar to previous paths, thereby increasing the diversity of paths.

2) Elite Strategy

In the traditional pheromone update rule, the uniform update strategy applied to all paths lacks differentiation, which results in slower convergence of the algorithm. Therefore, the convergence efficiency of the proposed algorithm is improved with the centralized pheromone updates on some excellent paths, speeding up the search process for the optimal solution. In this strategy, only the best partial routes from the current generation are reinforced with pheromone updates. In the i_{th} iteration, there are M ants in total, each ant k has a route length of L_k, and the algorithm selects the top M_e routes (elite routes) that performed the best for pheromone updates. M_e represents the number of elite paths, and we choose the shortest top 20% as elite paths, defined as: $M_e=max(1,[0.2M])$ The pheromone update method is as follows:

$$\tau_{ij}(t+1) = (1-\rho) \cdot \tau_{ij}(t) + \sum_{k=1}^{M_e} \delta_{ij}^k \cdot \frac{Q}{L_k} \tag{12}$$

where δ_{ij}^k is an indicator function. If path k passes through the edge (i, j), then $\delta_{ij}^k=1$; otherwise, $\delta_{ij}^k=0$.

3)The Step of Improved Ant Colony Optimization Algorithm

The operational framework of IACO for power inspection path optimization is illustrated in Fig. 2.

IV. RESULTS AND ANALYSIS

According to the layout map of the transmission towers in a city, the reliability and rationality of the algorithm are verified and analyzed through simulation experiments.

A. Actual Environment Description

Fig. 3 illustrates the distribution of transmission towers in a city, which are located in remote areas and distributed in the suburbs of cities, meeting the requirements of the ideal model established above. We select 20 towers in this area for the

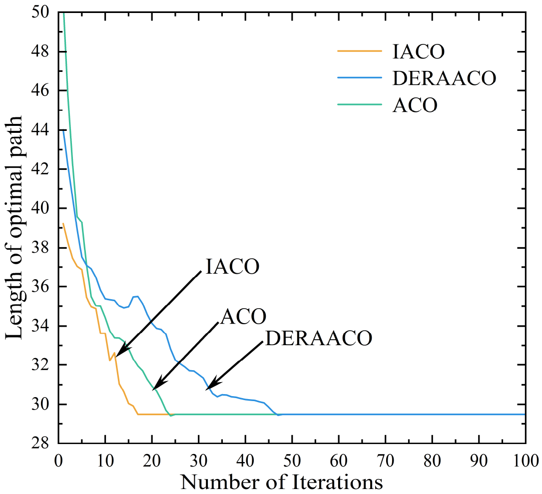

Fig. 7. Convergence Curves of Different Algorithms.

TABLE V
SIMULATION RESULTS FOR DIFFERENT ANT NUMBERS

Number of ants	Minimum distance/m	Running time/s
10	3493.912	1.562
20	3493.721	2.032
30	3493.144	2.763
50	3492.875	4.126
75	3492.674	6.158
100	3492.529	7.342
150	3492.529	10.753

experiment and obtain their plane coordinates on the map (Table II). Each tower is assigned a randomly generated number, which is not related to the tower's sequence.

B. Experimental Results and Analysis

1) 20×20 Obstacle Avoidance Area Simulation

The proposed IACO is compared with several well-performing algorithms involving the original ACO, dynamic evaporation rate adaptive ant colony optimization (DERAACO) [17], and the A* algorithm to verify its appealing performance. A standardized grid-based simulation framework was established to ensure experimental comparability. The navigation terrain was configured as a 400-cell lattice (20×20 resolution) with diagonally symmetric node placement - initial coordinates at (0.5, 19.5) and terminal coordinates at (19.5, 0.5). This orthogonal configuration eliminates directional bias while maintaining uniform path-search complexity across all algorithmic implementations. Due to the complexity of the actual inspection area environment, we modify the simulated testing environment based on the grid environment, aiming to enhance the practicality of the algorithm. Precisely, the proposed IACO is compared with A* algorithms to assess its effectiveness in route optimization, with the corresponding paths depicted in Fig. 4(a) and (b). Table III reports the corresponding results.

In this experiment, the algorithm initially fails to converge in the early iterations, and the result fluctuates constantly. Algorithmic stability improves monotonically with iteration progression. At 23 iterations, the optimal optimization effect

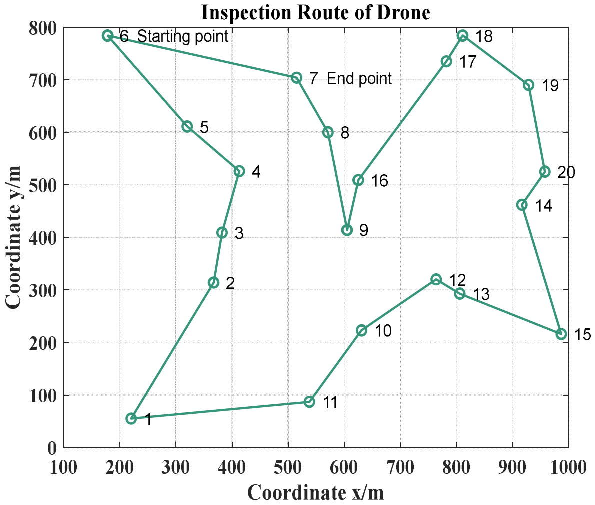

(a) Path Map of the IACO

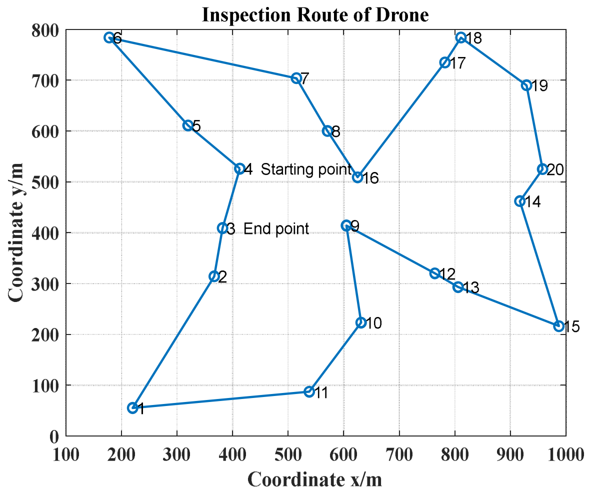

(b) Path Map of the Genetic Algorithm

Fig. 8. Drone Inspection Path Map

has been achieved, and the whole operation stabilizes. The findings indicate that the vehicle's path length, while navigating through the obstacle-filled area, measured 29.5 km.

Table III highlights that IACO has a 1% shorter path length than the A* algorithm. Regarding search efficiency (number of iterations), IACO improves by 80% compared to the A* algorithm, while for the number of turns, IACO has 8.3% less than the A* algorithm. Notably, the A* and proposed algorithms obtain the optimal solution. IACO demonstrates superior convergence efficiency, optimized path length, and enhanced robustness compared to the A* algorithm.

In Fig. 4, the black area represents obstacles, while the area indicates the regions where the inspection vehicle can pass. A collision-free path graph is obtained using the algorithm proposed in this paper for obstacle avoidance path planning. For 200 iterations and 80 ants, Fig. 5 compares the corresponding convergence curves.

To objectively evaluate the proposed algorithm's efficacy, comparative assessments were conducted against two benchmark algorithms: the original ACO and dynamic evaporation rate adaptive ant colony optimization (DERAACO). Accounting for the stochastic nature of probabilistic optimization algorithms, 30 independent trials were executed under identical conditions to ensure statistical

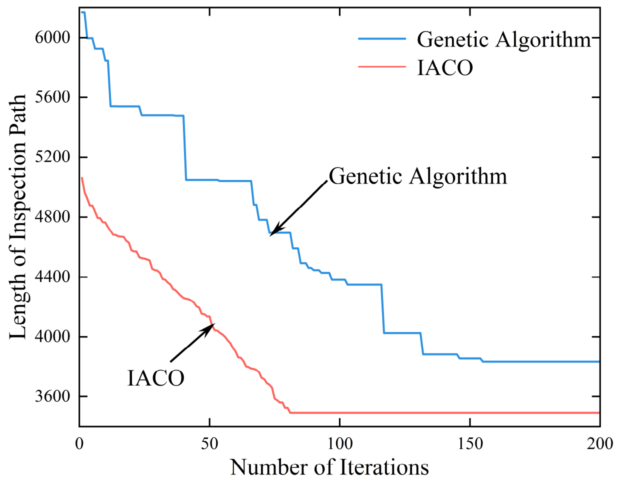

Fig. 9. Convergence Results

TABLE VI
SIMULATION RESULTS FOR DIFFERENT ITERATIONS

Number of iterations	Minimum distance/m	Running time /s
40	4259.784	2.037
60	4108.532	2.270
80	3791.360.	3.035
100	3492.529	3.237
150	3492.529	5.238
200	3492.529	10.296

reliability. The optimal path length (expressed as Best), average path length (expressed as Mean), standard deviation (expressed as Std), and other indicators are used to evaluate the performance. The optimal path of the model is shown in Fig. 6, while the convergence curves for the three ACOs are illustrated in Figure 7.Table IV summarizes the statistical outcomes of the optimal paths achieved by all the algorithms.

As demonstrated in Table IV, the Improved Ant Colony Optimization (IACO) exhibits comprehensive advantages in path-planning performance. Regarding optimal path length, IACO achieves parity with ACO and DERAACO at 29.5 units, outperforming the A* algorithm (29.8 units) by a 1.01% reduction. Statistically, IACO dominates in both central tendency and dispersion metrics: its mean path length (29.5) surpasses ACO (29.8), DERAACO (30.04), and A* (31.87), while its standard deviation (0) reflects absolute consistency, representing 100% reductions compared to DERAACO (0.66) and ACO (0.95). These metrics confirm IACO’s superior robustness and solution stability. In maneuverability optimization, IACO reduces turn counts to 11 on optimal paths, yielding 8.3%, 15.4%, and 26.7% improvements over ACO (12), DERAACO (13), and A* (15), respectively. Convergence analysis further highlights IACO’s computational efficiency: it attains optimal solutions in 18 iterations, 21.7% and 61.7% faster than ACO (23) and DERAACO (47). The mean convergence iteration (18.33 ± 0.22) demonstrates significantly tighter dispersion than ACO (25.30 ± 0.95) and DERAACO (49 ± 0.66), underscoring its algorithmic stability. Collectively, these results validate

TABLE VII
EACH ALGORITHM OPTIMIZES THE SHORTEST DISTANCE

Algorithm	Genetic algorithm		The algorithm in this article	
Number	*Optimal value/m*	*Running time/s*	*Optimal value/m*	*Running time/s*
1	3561.242	9.71	3492.529	7.34
2	3541.514	9.57	3492.529	7.51
3	3671.660	9.75	3492.529	7.30
4	3636.478	9.76	3492.529	7.68
5	3525.035	9.68	3492.529	7.42
6	3677.582	9.80	3492.529	7.43
7	3708.115	9.91	3492.529	7.52
8	3500.647	9.56	3492.529	7.61
9	3570.098	9.67	3492.529	7.38
10	3525.525	9.68	3492.529	7.55
Average value	3591.790	9.71.	3492.529	7.47

IACO’s triple advancements in solution quality, computational efficiency, and operational reliability.

2) Drone Inspection Area Simulation

The number of towers in the drone inspection area is 20, and the parameters are set to α=1.5, β=2, ρ=0.1, and Q=k100. The initial population size of the genetic algorithm is 2000, the chromosome gene dimension is 31, and the maximum number of generations is 1000. The inspection route starts from the initial point. Each tower is passed once without repetition or returning, and the drone returns to the starting point. The simulation results are presented next.

The best inspection path is presented in Fig. 8, with Fig. 8(a) depicting the path planning results of the proposed method and Fig. 8(b) the genetic algorithm path planning results. The position of each transmission tower is presented in a blue hollow point, and the number on each point is the tower's serial number. The inspection-specific path order is 6 →5→4→3→2→1→11→10→12→13→15→14→20→19 →18→17→16→9→8→7. The path traverses all towers without repetition.

Fig. 9 compares the performance of the genetic algorithm (blue curve) and IACO (red curve) based on the number of iterations and the length of the inspection path. The results show that the proposed algorithm converges faster. The drone inspection path is 3492.529 m, and the total inspection path length is 32.992529 km.

To compare the performance difference, we modify the value of the parameters. Table V reports the simulation results for 200 iterations while modifying the number of ants. Table VI presents the results for 100 ants under various number of iterations.

Tables V and VI infer that changing the number of ants and iterations significantly impacts the simulation results. When the number of ants is 100, the shortest distance of path

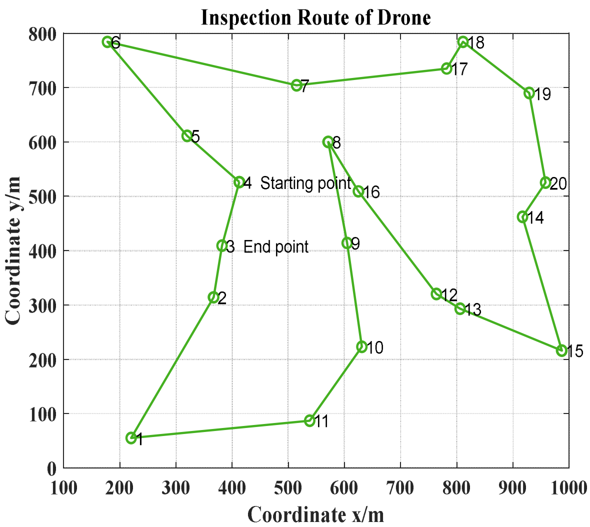

(a) Path Map of ACO

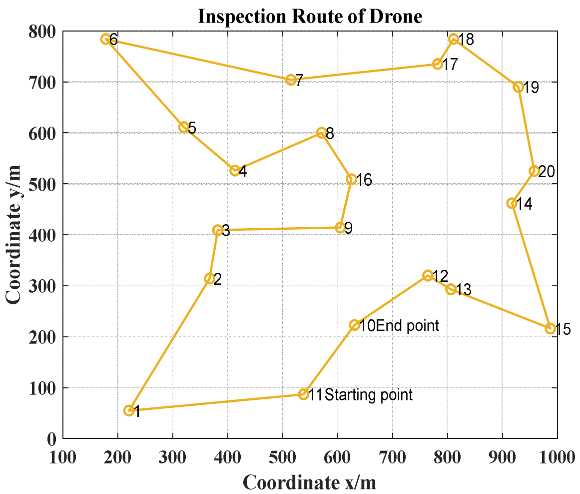

(b) Path Map of DERAACO

Fig. 10. Drone Inspection Path Map

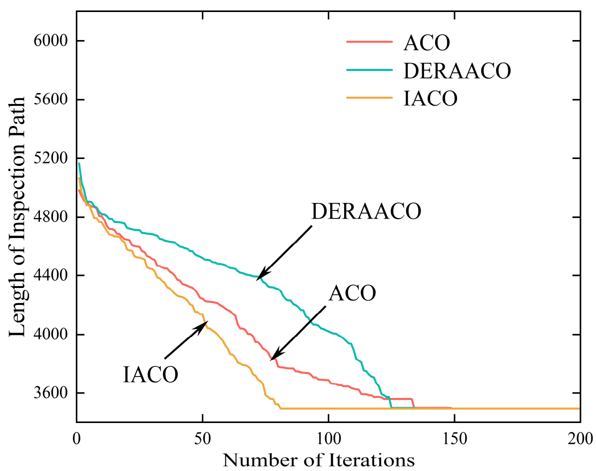

Fig. 11. Convergence Results

planning reaches the convergence value (3492.529 m), and the running time is 7.342 s, which has a higher solution quality than using a smaller number of ants (such as 30 or 50). At the same time, although a more significant number of ants (such as 150) can be used, the running time will increase significantly. When the number of iterations is 100, the shortest distance of path planning stabilizes (3492.529 m),

TABLE VIII
EXPERIMENTAL RESULTS OF DIFFERENT ALGORITHMS

Algorithm	Minimum distance/m	Average distance/m	Variance	Running time /s
ACO	3492.529	3517.673	2.777	9.386
DERAACO	3492.529	3532.428	6.148	11.528
IACO	3492.529	3502.509	1.281	6.199

and the running time is 3.237 s. This setting provides a better path solution than a smaller number of iterations (such as 40 or 60), while further increasing the number of iterations (such as 150 or 200) does not improve the path length but significantly increases Run time. Therefore, 100 iterations balance quality and computational efficiency. Hence, considering the solution quality and operation efficiency, the optimal settings are 100 ants and 100 iterations.

Table VII presents the experimental results from 10 independent runs of each algorithm, suggesting that the optimized path distance of the proposed algorithm is shorter than that of the genetic algorithm, demonstrating the superiority of our method. Regarding the running time of each algorithm, superiority of our method. The proposed algorithm exhibits significantly improved computational efficiency compared to traditional genetic algorithms, achieving faster execution times while maintaining solution quality. Furthermore, the running highlights that the proposed algorithm consistently produces the same results, whereas the genetic algorithm shows some variability, indicating better stability for the proposed algorithm.

ACO and DERAACO are compared with IACO to verify the optimization performance further. The best inspection path is depicted in Fig. 10, with Fig. 10(a) and Fig. 10(b) presenting the ACO and DERAACO path planning results, respectively. The convergence results are illustrated in Fig. 11. It can be observed that all algorithms exhibit a decreasing trend in path length as iterations increase, demonstrating their ability to optimize the solution over time. Among the three, IACO consistently achieves the shortest path length and converges faster than the other methods. ACO performs moderately, while DERAACO provides intermediate results, indicating a balance between optimization speed and solution quality.

In the simulation experiment, the three algorithms are executed 20 times, and the minimum value, average value, variance, and running time of the above results are used for comparison. The corresponding results are reported in Table VIII, highlighting that IACO has better optimization ability. Its minimum and average values and variance are the smallest, indicating that IACO has better stability than ACO and DERAACO. In general, the solution quality of the developed IACO algorithm is the best, and its running time is also better than ACO and DERAACO. Thus, it can effectively improve the comprehensive optimization performance of solving power inspection problems.

V. CONCLUSION

This study has demonstrated the effectiveness of the proposed inspection system model and the improved ant colony optimization algorithm (IACO) in addressing the challenges of power inspection. By integrating an advanced obstacle avoidance strategy with the IACO algorithm, the framework offers a reliable and effective solution for optimizing path planning in intricate power grid environments. IACO introduces a multi-path selection mechanism and elite strategy, and its performance is evaluated through effectiveness verification. Combined with practical inspection, the constraint conditions in an inspection are studied, and the mathematical model and objective function are established. The simulation experiments are carried out in 20×20 grid environments, and the actual transmission towers are considered the experimental objects. The performance of the proposed algorithm is validated through experimental simulations conducted in MATLAB.

To validate its outstanding performance in power inspection path planning, IACO is challenged against several advanced algorithms, including the original ACO, dynamic evaporation rate adaptive ant colony optimization (DERAACO), A* algorithm, and genetic algorithm. The comprehensive statistical analysis shows that IACO provides superior path-planning solutions, offering benefits in terms of path length, convergence rate, and number of turns.

Thus, the proposed algorithm demonstrates an appealing performance in power inspection path planning in complex environments. Future works will focus on improving path-planning techniques and inspection efficiency. IACO provides theoretical guidance for the power company in formulating inspection plans.

REFERENCES

[1] F. L. He, J. Q. Chen, Q. H. Li, Y. Q. Yi, and Y. J. Zhang, “Application and development of internet of things technology in smart grid,” *Power System Protection and Control*, vol. 48, no. 3, pp. 58-69, 2020.

[2] G. W. Shao, Z. Liu, J. Fu, J. Y. Tan, Y. Chen, and L. W. Zhou, “Research progress in unmanned aerial vehicle inspection technology on overhead transmission lines,” *High Voltage Engineering*, vol. 46, no. 1, pp. 14-22, 2020.

[3] Z. Li, Q. Wang, T. Zhang, C. Ju, S. Suzuki and A. Namiki, “UAV High-Voltage Power Transmission Line Autonomous Correction Inspection System Based on Object Detection,” *IEEE Sensors Journal*, vol. 23, no. 9, pp. 10215-10230, 2023.

[4] Y. D. Yong, Y. Q. Wang, C. Gao, H. Q. Cai, S. P. Cao, and Q. Fan, “Intelligent path planning method for unmanned serial vehicle inspection of power transmission lines,” *Journal of Chongqing University of Technology (Natural Science)*, vol. 37. no. 9, 2023.

[5] S. Lu, Y. Zhang, and J. Su, “Mobile robot for power substation inspection: A survey,” *IEEE/CAA Journal of Automatica Sinica,* vol. 4, no. 4, pp. 830-847, 2017.

[6] Yang M X. “Comparison of several methods of transmission line inspection analysis of advantage of unmanned helicopter inspection,” *Smart Grid*, vol. 05, no. 3, pp. 148-154, 2015.

[7] W. G. Chen, X. G. Hu, X. Zheng, Z. X. Ma, and H. Chen, “Optimization of traveling track of inspection robot in substation based on improved genetic algorithm,” *Guangdong Electric Power*, vol. 34, no. 06, pp. 48-54, 2021.

[8] Y. X. Lu, Y. B. Wei, Q. C. Zhao, and S. C. Li, “Path planning of a power emergency robot based on an analytic hierarchy process and improved A* algorithm,” *Power System Protection and Contro*l, vol. 49, no. 09, pp. 82-89, 2021.

[9] Z. W. Xie, Z. Wang, R. Wang, and Y. Zhou, “Study on path planning of substation inspection robot based on improved ant colony algorithm,” *China Energy and Environmental Protection,* vol. 43, no. 12, pp. 212-216, 2021.

[10] Z. Huang, H. X. Wang, T. P. Zhang, and B. Yu, “The collaborative power inspection task allocation method of unmanned aerial vehicle and operating vehicle,” *IEEE Access*, vol. 9, pp. 62926-62934, 2021.

[11] M. Zhao, B. Zhang, X. P. Hu, and M. F. Huang, “Cooperative Operation Optimization for Transmission Inspection with Vehicle-Mounted UAV,” *Journal of Systems&Management*, vol. 31, no. 6, pp. 1098-1108, 2022.

[12] Xiaoxia Zhang, Ziqiao Yu, Yinyin Hu, and Jiao Yang, “Milling Force Prediction of Titanium Alloy Based on Support Vector Machine and Ant Colony Optimization,” *IAENG International Journal of Computer Science*, vol. 48, no.2, pp223-235, 2021.

[13] Hongbo Li, Xiaoxia Zhang, Shuai Fu, and Yinyin Hu, “A Hybrid Algorithm Based on Ant Colony Optimization and Differential Evolution for Vehicle Routing Problem,” *Engineering Letters*, vol. 29, no.3, pp1201-1211, 2021.

[14] M Dorigo, Maniezzo V, and Colorni A, “Ant system: optimization by a colony of cooperating agents,” *IEEE Transactions on Systems, Man, and Cybernetics, Part B (Cybernetics),* vol. 26, no. 1, pp. 29-41, 2002.

[15] A.L. Amith, Amrinder Singh, H.N. Harsha, N. R. Prasad, and Lakshmi Shrinivasan, “Normal Probability and Heuristics based Path Planning and Navigation System for Mapped Roads,” *Procedia Computer Science*, vol. 89, pp. 369-377, 2016.

[16] ROBERTI R, and RUTHMAIR M, “Exact methods for the traveling salesman problem with drone,” *Transportation Science,* vol. 55, no. 5, pp. 315-335, 2021.

[17] SHEN D. F. Shen, B. L. Wang, X. F. Li, P. F. Bai, “Automatic fabric drop trolley path planning based on improved ant colony algorithm,” *Journal of Xi'an Polytechnic University*, vol. 38, no. 1, pp. 50-59, 2024.

Lei Tian completed his Master’s in Mobile Communication at Xi’an University of Science and Technology in 2006. He received his Ph.D. in Optoelectronic Integrated Circuit Design (OEIC) from Xidian University in 2015, followed by postdoctoral research at Northwest University in 2019. His primary research interests encompass analog and mixed-signal integrated circuits, optoelectronic signal processing, optocouplers, SOC design, and infrared communication technologies.

Minhang Mao received her Bachelor's degree in Electronic Information Engineering from Hefei Normal University in 2020. And then she entered Xi'an University of Posts and Telecommunications to pursue a master's degree in 2022. Her main research interests are the intelligent algorithm in electric power system.

Baoyu Hou received his B.E. degree in Electric Engineering & Automation from North China Electric Power University. And then, he has been working in the Quzhou Power Supply Company of the State Grid Zhejiang Electric Power Corporation. He is mainly responsible for scientific research projects of the Ministry of Science and Technology and the Department of Digitalization, and his main responsibilities are smart power and digital grid design.

Gao Ma received his Master degree in Geographic Information Systems at Shaanxi Normal University in 2015. Then he engaged in research on BD satellite applications and vegetation remote sensing data processing at the CAST Xi’an Institute of Space Radio Technology, China Academy of Space Technology.